Transverse shear stiffness of a chevron folded core used in sandwich construction

Arthur Lebée, Karam Sab

Transverse Shear Stiffness of a Chevron Folded Core Used in Sandwich Construction

A. Lebée, K. Sab*

Université Paris-Est. UR Navier. École des Ponts ParisTech,
6 et 8 avenue Blaise Pascal.
77455 Marne-la-Vallée cedex2
tel.+33-1-64153749, fax.+33-1-64153741,
e-mail: arthur.lebee@lami.enpc.fr, sab@enpc.fr

Abstract

Using Kelsey, Gellatly, and Clark (1958) unit load method, upper and lower bounds for the effective transverse shear moduli of a chevron folded core used in sandwich construction are analytically derived and compared to finite element computations. We found that these bounds are generally loose and that in some cases chevron folded cores are 40% stiffer than honeycomb-like cores.

Key words: Sandwich panels, Folded cores, Effective transverse shear modulus, Chevron pattern.

1. Introduction

Sandwich panels made of two thin skins separated by a thick periodic core structure are commonly used in many engineering applications. They offer a good compromise between strength and weight which is especially important in aeronautics.

When bending the sandwich panel, the skins are subjected to in-plane traction and compression whereas the core is subjected to transverse shear. Many constituents can be used as core materials. Balsa glued between stiffer pieces of wood was one of the first attempts to make a sandwich panel. Nowadays, organic compound foams (such as polyurethane foam) used with metallic skins are widespread in buildings as insulating panels. Phenolic paper honeycomb is extensively used in aeronautic structures.

Recently, new types of promising cores have emerged. Truss core panels using new welding techniques are raising interest because of their strength (Wicks and Hutchinson, 2001; Wadley, 2002; Cote et al., 2007). Folded cores are promising because of new production means (Basily and Elsayed, 2004b; Nguyen et al., 2005a; Heimbs et al., 2006; Kintscher et al., 2007). Among them, the chevron folded core was probably the first to be manufactured (Fig. 1).

It seems that chevron folded core manufacturing was first considered at the beginning of the 20^{th} century. Later, the pattern was under investigation in Kazan University. More recently, continuous production and several new techniques have emerged (Kling, 2005; Basily and Elsayed, 2006, 2004a; Kehrle,

2004).The strength of chevron folded cores has been experimentally investigated by Basily and Elsayed (2004b), Kintscher et al. (2007) and Nguyen et al. (2005a) and it has been numerically simulated by Nguyen et al. (2005a), Heimbs et al. (2006) and Heimbs (2009). Moreover, their transverse shear stiffness has been experimentally investigated by Kintscher et al. (2007) but, to the authors knowledge, no theoretical work has been done yet.

The aim of this paper is to derive bounds for the transverse shear stiffness of chevron folded cores. Kelsey et al. (1958) first suggested a method for deriving such bounds for honeycomb-like cores. One may refer also to Gibson and Ashby (1988) for a detailed description of this method. Since then, many honeycomb geometries have been assessed (Hohe and Becker, 2002; Xu et al., 2001). New homogenization methods have been suggested. For instance, Hohe (2003) suggested the application of *ad hoc* boundary conditions reproducing transverse strain loading $\varepsilon_{\alpha 3}$ to a unit cell of the sandwich panel, including the skins, so that the interaction between the core and the skins was taken into account. Chen and Davalos (2005) suggested a semi-analytical approach in order to refine Kelsey et al. (1958) analysis close to the skins.

Yet, as a first attempt to determine the transverse shear stiffness of folded chevron, it seems relevant to use Kelsey et al. (1958) approach. Even if only bounds will be derived, it offers a quick and comprehensive view of chevron pattern stiffness, enables us to look for most efficient configurations and leads to exact solutions when bounds are equal.

The paper is organized as follows: Section 2 is devoted to the geometric description of the chevron pattern and the suggested analytical bounds are derived in Section 3. In order to assess the validity of these bounds, a finite element analysis on a representative unit cell is performed in Section 4. The final section gives an insight into future works.

2. The chevron pattern homogenized as Mindlin-Reissner plate model

Like honeycomb, the chevron pattern is periodic in the in-plane directions. Four identical parallelogram - shape faces are necessary to generate the whole pattern by periodicity along the $\underline{e}_1$ vector (period $2a$) and the $\underline{e}_2$ vector (period $2s$) where $\mathcal{M} = (A, \underline{e}_1, \underline{e}_2, \underline{e}_3)$ is the main coordinate system. Fig. 2-a shows these faces: Face 1= $ABCD$, Face 2= $D'CBA'$, Face 3= $A'''B''CD'$ and Face 4 = $DCB''A''$.

Table 1 gives the vertices' coordinates in terms of four geometric parameters: a, s, v and h where v is a horizontal offset parameter ($v = 0$ when B is aligned with A and A') and h is the pattern height.

Actually, several parameter sets have been suggested for the geometric description of the chevron pattern (Basily and Elsayed, 2004a; Zakirov et al., 2008). Among them, the set a_0, b_0, δ, ζ fully determines the geometry and the position of Face 1. Face 1 is a parallelogram (a_0 and b_0 are the side lengths) which is tilted by angles δ and ζ with respect to the main coordinate system, as shown in Figure 2-b.

Vertex	A	B	C	D	A'	D'	A''	B''	A'''
x_1	0	v	$a+v$	a	0	a	$2a$	$2a+v$	$2a$
x_2	0	s	s	0	$2s$	$2s$	0	s	$2s$
x_3	0	0	h	h	0	h	0	0	0

Table 1: Vertices' coordinates

- δ is the *member angle* by analogy with truss beams: cutting the chevron pattern by the $(A, \underline{e}_1, \underline{e}_3)$ plane gives a zigzag shape similar to that of a Warren-type truss beam.
- ζ is the *closure angle* equal to the half angle between Face 1 and Face 2 along the BC edge. For $\zeta = 0$, the pattern is completely folded and for $\zeta = \pi/2$, the pattern is prismatic.
- $\beta_0 = \arctan\left(\frac{\tan\delta}{\cos\zeta}\right)$ is $\widehat{DAB}$ angle
- $\alpha = \arctan\left(\frac{1}{\tan\zeta\sin\delta}\right)$ is $\widehat{A'AB}$ angle

We have:

$$\begin{aligned} a &= a_0\cos\delta, \\ s &= b_0\cos\alpha, \\ v &= b_0\sin\alpha, \\ h &= a_0\sin\delta. \end{aligned}$$

The chevron pattern has actually three major symmetries. When used as a core between two isotropic skins, these symmetries lead to several simplifications in the Reissner-Mindlin plate constitutive law (Reissner, 1985). The fully coupled constitutive law can be summerized as follows:

$$\left(\begin{array}{c} N_{11} \\ N_{22} \\ N_{12} \\ \hline M_{11} \\ M_{22} \\ M_{12} \\ \hline Q_1 \\ Q_2 \end{array}\right) = \left(\begin{array}{ccc|ccc|cc} A_{11} & A_{12} & A_{13} & B_{11} & B_{21} & B_{31} & K_{11} & K_{12} \\ A_{12} & A_{22} & A_{23} & B_{12} & B_{22} & B_{32} & K_{21} & K_{22} \\ A_{13} & A_{23} & A_{33} & B_{13} & B_{23} & B_{33} & K_{31} & K_{32} \\ \hline B_{11} & B_{12} & B_{13} & D_{11} & D_{12} & D_{13} & L_{41} & L_{42} \\ B_{21} & B_{22} & B_{23} & D_{12} & D_{22} & D_{23} & L_{51} & L_{52} \\ B_{31} & B_{32} & B_{33} & D_{13} & D_{23} & D_{33} & L_{61} & L_{62} \\ \hline K_{11} & K_{21} & K_{31} & L_{41} & L_{51} & L_{61} & F_{11} & F_{12} \\ K_{12} & K_{22} & K_{32} & L_{42} & L_{52} & L_{62} & F_{12} & F_{22} \end{array}\right) \cdot \left(\begin{array}{c} e_{11} \\ e_{22} \\ 2e_{12} \\ \hline \chi_{11} \\ \chi_{22} \\ 2\chi_{12} \\ \hline \gamma_1 \\ \gamma_2 \end{array}\right) \tag{1}$$

where $N_{\alpha\beta}$ are the membrane generalized stress components, $M_{\alpha\beta}$ are the bending moment components, Q_α are the shear forces, $e_{\alpha\beta}$ are the in-plane strains, $\chi_{\alpha\beta}$ are the curvatures and γ_α are the out-of-plane

shear strains. Generalized strains are illustrated on Fig. 3. A_{ij}, B_{ij} and D_{ij} are the usual Love-Kirchhoff plate stiffnesses. $F_{\alpha\beta}$ is the usual Reissner shear stiffness. $K_{\alpha i}$ and $L_{\alpha i}$ are a possible couplings between ($N_{\alpha\beta}$, $M_{\alpha\beta}$) and Q_α.

Due to the rotational symmetry $\mathcal{S}$ of axis $(S, \underline{e}_3)$, shown in Fig. 4-a, we have $K_{\alpha i} = L_{\alpha i} = 0$. Fig. 4-b shows the central symmetry $\mathcal{R}$ with respect to the center point of Face 1, R. This symmetry uncouples membrane stresses and flexural stresses: $B_{ij} = 0$ (similar to mirror symmetry for laminates). Fig. 4-c shows the symmetry $\mathcal{N}$ with respect to the $(B, \underline{e}_1, \underline{e}_3)$ plane. This symmetry sets $A_{13} = A_{23} = D_{13} = D_{23} = F_{12} = 0$. Thus, it uncouples transverse shear stresses. Taking into account all uncouplings leads to the following constitutive law:

$$\left(\begin{array}{c} N_{11} \\ N_{22} \\ N_{12} \\ \hline M_{11} \\ M_{22} \\ M_{12} \\ \hline Q_1 \\ Q_2 \end{array}\right) = \left(\begin{array}{ccc|ccc|cc} A_{11} & A_{12} & 0 & 0 & 0 & 0 & 0 & 0 \\ A_{12} & A_{22} & 0 & 0 & 0 & 0 & 0 & 0 \\ 0 & 0 & A_{33} & 0 & 0 & 0 & 0 & 0 \\ \hline 0 & 0 & 0 & D_{11} & D_{12} & 0 & 0 & 0 \\ 0 & 0 & 0 & D_{12} & D_{22} & 0 & 0 & 0 \\ 0 & 0 & 0 & 0 & 0 & D_{33} & 0 & 0 \\ \hline 0 & 0 & 0 & 0 & 0 & 0 & F_{11} & 0 \\ 0 & 0 & 0 & 0 & 0 & 0 & 0 & F_{22} \end{array}\right) \cdot \left(\begin{array}{c} e_{11} \\ e_{22} \\ 2e_{12} \\ \hline \chi_{11} \\ \chi_{22} \\ 2\chi_{12} \\ \hline \gamma_1 \\ \gamma_2 \end{array}\right) \tag{2}$$

The symmetries described above are respectively associated with the following matrices in the reference frame $(\underline{e}_1, \underline{e}_2, \underline{e}_3)$:

$$\underline{\underline{\mathcal{R}}} = \begin{pmatrix} -1 & 0 & 0 \\ 0 & -1 & 0 \\ 0 & 0 & -1 \end{pmatrix}, \quad \underline{\underline{\mathcal{N}}} = \begin{pmatrix} 1 & 0 & 0 \\ 0 & -1 & 0 \\ 0 & 0 & 1 \end{pmatrix}, \quad \underline{\underline{\mathcal{S}}} = \begin{pmatrix} -1 & 0 & 0 \\ 0 & -1 & 0 \\ 0 & 0 & 1 \end{pmatrix}. \tag{3}$$

It is useful to introduce a local basis $\mathcal{L}^k = (\underline{e}^k_u, \underline{e}^k_v, \underline{e}^k_w)$ associated to Face k ($k = 1, 2, 3, 4$) as shown in Figure 2. For Face 1, vector $\underline{e}^1_u$ is along the AD edge, $\underline{e}^1_w$ is normal to the face with $\underline{e}^1_w \cdot \underline{e}_3 > 0$ and $\underline{e}^1_v$ is such that $\mathcal{L}^1$ is direct. Thus, the components of $(\underline{e}^1_u, \underline{e}^1_v, \underline{e}^1_w)$ in the $(\underline{e}_1, \underline{e}_2, \underline{e}_3)$ basis are given by:

$$(\underline{e}^1_u, \underline{e}^1_v, \underline{e}^1_w) = \begin{pmatrix} \cos\delta & \sin\zeta\cos\delta & -\sin\delta\sin\zeta \\ 0 & \sin\zeta & \cos\zeta \\ \sin\delta & -\cos\delta\cos\zeta & \cos\delta\sin\zeta \end{pmatrix}_{(\underline{e}_1, \underline{e}_2, \underline{e}_3)}. \tag{4}$$

Moreover, the symmetry matrices enables the determination of the components of the other local basis $\mathcal{L}^2$, $\mathcal{L}^3$ and $\mathcal{L}^4$ as detailed in the appendix.

In sandwich panels, the membrane and flexural moduli are usually derived assuming that the core structure does not contribute to the overall stiffness. It is also assumed for transverse shear stiffness that $F_{\alpha\alpha} = hG_{\alpha 3}$ where G is the effective shear stiffness of the core. Finally, regarding shear behavior, there are only two transverse shear moduli to determine: G_{13} and G_{23}.

3. Analytical bounds

According to the approach of Kelsey et al. (1958), the minimum potential energy theorem is used to derive upper bounds for the effective transverse shear modulus in the $\alpha-$ direction, $G_{\alpha 3}$. A uniform horizontal displacement $h\gamma_{\alpha 3}$ in the $\alpha-$direction is imposed on the top face of the core material while its lower face is fixed. Here, $\alpha = 1, 2$ are the in-plane directions, $\gamma_{\alpha 3}$ is the out-of-plane shear strain in the $\alpha-$direction and h is the height of the core. Then, the normalized strain energy of any trial strain field which is piecewise uniform in the core walls and compatible with the kinematic boundary conditions provides an upper bound for $G_{\alpha 3}$, noted $G^{+}_{\alpha 3}$. Similarly, the minimum complementary energy theorem is used for deriving lower bounds for $G_{\alpha 3}$. A uniform horizontal stress load $\tau_{\alpha 3}$ (respectively, $-\tau_{\alpha 3}$) is applied in the $\alpha-$direction to the upper (respectively, lower) face of the core material. Then, the normalized stress energy of any piecewise uniform trial stress field which is statically compatible with the boundary conditions provides a lower bound for $G_{\alpha 3}$, noted $G^{-}_{\alpha 3}$.

3.1. Lower bounds

A uniformly distributed horizontal force per unit length, $\underline{f}^{\pm}$, is applied to the upper $(-)$ and lower edges $(+)$ of the pattern. Fig. 5-a shows $\underline{f}^{\pm}$ for transverse shear loading in direction 1, τ_1:

$$\underline{f}^{\pm} = \pm 2 \frac{a\, s}{b_0} \tau_1 \underline{e}_1 \ , \tag{5}$$

and Fig. 5-b shows $\underline{f}^{\pm}$ for transverse shear loading in direction 2, τ_2:

$$\underline{f}^{\pm} = \pm 2 \frac{a\, s}{b_0} \tau_2 \underline{e}_2 . \tag{6}$$

Piecewise uniform plane stress is assumed for each face. Hence, the stress of Face 1 writes:

$$\underline{\underline{\sigma}}^1 = \sigma^1_{uu} \underline{e}^1_u \otimes \underline{e}^1_u + \sigma^1_{vv} \underline{e}^1_v \otimes \underline{e}^1_v + \sigma^1_{uv} \left(\underline{e}^1_u \otimes \underline{e}^1_v + \underline{e}^1_v \otimes \underline{e}^1_u \right) \tag{7}$$

where $\otimes$ is the dyadic product of two vectors and σ^1_{uu}, σ^1_{vv}, σ^1_{uv} are three unknowns to be determined. Thanks to $\mathcal{N}$ and $\mathcal{S}$ symmetries of the pattern and the considered loadings, it is possible to express the stress $\underline{\underline{\sigma}}^k$ of Face k, $k = 2, 3, 4$, in terms of $\underline{\underline{\sigma}}^1$. Indeed, the following relations are easily derived:

$$\underline{\underline{\sigma}}^2 = \epsilon \underline{\underline{\mathcal{N}}}\, \underline{\underline{\sigma}}^1 \underline{\underline{\mathcal{N}}}, \qquad \underline{\underline{\sigma}}^4 = -\underline{\underline{\mathcal{S}}}\, \underline{\underline{\sigma}}^1 \underline{\underline{\mathcal{S}}}, \qquad \underline{\underline{\sigma}}^3 = \epsilon \underline{\underline{\mathcal{N}}}\, \underline{\underline{\sigma}}^4 \underline{\underline{\mathcal{N}}}, \tag{8}$$

where $\epsilon = 1$ for loading in direction 1 and $\epsilon = -1$ for loading in direction 2.

The equilibrium condition at edge AD (or edge BC) is written as:

$$\underline{\underline{\sigma}}^1 \cdot \underline{e}^1_v + \underline{\underline{\sigma}}^2 \cdot \left(-\underline{e}^2_v \right) = \underline{0} \tag{9}$$

Similarly, the equilibrium condition at edge CD (or edge AB) writes:

$$-t \left(\underline{\underline{\sigma}}^1 \cdot \underline{n}^1 + \underline{\underline{\sigma}}^4 \cdot \underline{n}^4 \right) + \underline{f}^{+} = 0 \tag{10}$$

where t is the faces' thickness and $\underline{n}^k$ is the outer normal of Face $k = 1, 4$ along CD ($\underline{n}^k$ belongs to Face k plane):

$$\underline{n}^1 = -\sin\beta_0 \underline{e}_u^1 + \cos\beta_0 \underline{e}_v^1 \qquad \underline{n}^4 = \sin\beta_0 \underline{e}_u^4 - \cos\beta_0 \underline{e}_v^4 \tag{11}$$

The six (non independent) linear equations (9-10) uniquely determine the three unknowns σ_{uu}^1, σ_{vv}^1, σ_{uv}^1. The solution is:

loading in direction 1:	loading in direction 2:
$\sigma_{uu}^1 = -\frac{a_0\tau_1}{t}\sin\zeta$	$\sigma_{uu}^1 = -\frac{a_0\tau_2}{t}\left(\frac{1}{\tan\delta} - \tan\delta\right)\cos\zeta\cos\delta$
$\sigma_{vv}^1 = 0$	$\sigma_{vv}^1 = 0$
$\sigma_{uv}^1 = 0$	$\sigma_{uv}^1 = -\frac{a_0\tau_2}{t}\cos\delta$

The faces' constitutive material is assumed to be isotropic[1]. Hence, the total stress energy of the unit cell is given by:

$$W_{int}^* = 2\sin\beta_0 b_0 a_0 t\left(\frac{2(1+\nu_s)}{E_s}(\sigma_{uv}^1)^2 + \frac{1}{E_s}(\sigma_{uu}^1)^2\right) \tag{12}$$

where E_s and ν_s are the solid Young modulus and Poisson's ratio. The stress energy of the effective core material subjected to the transverse shear stress τ_α in the direction α is:

$$W_{ext}^* = 2ahs\frac{\tau_\alpha^2}{G_{\alpha 3}}. \tag{13}$$

The theorem of the complementary energy states that $W_{ext}^* \leq W_{int}^*$. Inserting the expressions of σ_{uu}^1 and σ_{uv}^1 into (12) gives the lower bounds:

$$G_{13} \geq G_{13}^- = \frac{t}{a_0}E_s\ \frac{\sin\delta\cos\delta}{\sin\zeta},$$
$$G_{23} \geq G_{23}^- = \frac{t}{a_0}E_s\ \frac{\sin\delta}{\cos\delta}\ \frac{\sin\zeta}{2(1+\nu_s)+\left(\frac{1}{\tan\delta}-\tan\delta\right)^2\cos^2\zeta}.$$

It is more convenient to use the following normalization:

$$\mathcal{E}_\alpha = \frac{G_{\alpha 3}}{\rho G_s} \tag{14}$$

where ρ is the core relative density, G_s is the solid shear modulus and $\mathcal{E}_\alpha$ is the normalized transverse shear modulus in direction α. For chevron cores, ρ is given by:

$$\rho = \frac{t}{a_0\sin\zeta\sin\delta\cos\delta}. \tag{15}$$

Hence, we have:

$$\mathcal{E}_1 \geq \mathcal{E}_1^- = 2(1+\nu_s)\ \sin^2\delta\cos^2\delta,$$
$$\mathcal{E}_2 \geq \mathcal{E}_2^- = 2(1+\nu_s)\ \frac{\sin^2\delta\sin^2\zeta}{2(1+\nu_s)+\left(\frac{1}{\tan\delta}-\tan\delta\right)^2\cos^2\zeta}.$$

[1]This is the case for metallic cores and for Nomex paper core. For CFRP cores, anisotropy has to be introduced.

3.2. Upper bounds

In order to derive an upper bound for the transverse shear modulus $G_{\alpha 3}$, a relative horizontal displacement, $\gamma_\alpha h$, between the top and the bottom of the chevron pattern is prescribed in the direction α as shown in Fig. 5-(c,d). The corresponding overall transformation is:

$$\underline{\underline{F}} = \underline{\underline{I}} + \gamma_\alpha \underline{e}_\alpha \otimes \underline{e}_3 \tag{16}$$

where $\underline{\underline{I}}$ is the unit second order tensor.

The in-plane components of the uniform Green-Lagrange strain tensor of Face 1 with respect to the $(\underline{e}^1_u, \underline{e}^1_v)$ local basis are given by:

$$e^1_{\lambda\mu} = \frac{1}{2}\left(\underline{e}^{1*}_\lambda \cdot \underline{e}^{1*}_\mu - \delta_{\lambda\mu}\right) \qquad \lambda, \mu = u, v, \tag{17}$$

where $\underline{e}^{1*}_\lambda = \underline{\underline{F}} \cdot \underline{e}^1_\lambda$, and $\delta_{\lambda\mu}$ is the Krönecker symbol. Neglecting the second order terms in γ_α leads to the following linearized in-plane strain components:

loading in direction 1:	loading in direction 2:
$\varepsilon^1_{uu} = \gamma_1 \sin\delta\cos\delta$	$\varepsilon^1_{uu} = 0$
$\varepsilon^1_{vv} = -\gamma_1 \sin\delta\cos\delta\cos^2\zeta$	$\varepsilon^1_{vv} = -\gamma_2 \cos\zeta\sin\zeta\cos\delta$
$\varepsilon^1_{uv} = -\frac{\gamma_1}{2}\cos 2\delta\cos\zeta$	$\varepsilon^1_{uv} = \frac{\gamma_2}{2}\sin\zeta\sin\delta$

Piecewise uniform plane stress is assumed in each face. Therefore, the strain energy density of Face 1 is given by:

$$w = \frac{1}{2}\left(\frac{E_s}{1+\nu_s}\left((\varepsilon^1_{uu})^2 + (\varepsilon^1_{vv})^2 + 2(\varepsilon^1_{uv})^2\right) + \frac{\nu_s E_s}{1-\nu_s^2}\left(\varepsilon^1_{uu} + \varepsilon^1_{vv}\right)^2\right). \tag{18}$$

The total strain energy stored in the unit cell is:

$$W_{int} = 2\sin\beta_0 b_0 a_0 t w. \tag{19}$$

The strain energy stored in the effective core material is:

$$W_{ext} = 2ahsG_{\alpha 3}\gamma_\alpha^2. \tag{20}$$

According to the potential energy theorem, we have $W_{ext} \leq W_{int}$. Hence, the following upper bounds for the normalized transverse shear moduli are obtained:

$$\mathcal{E}_1 \leq \mathcal{E}_1^+ = \tfrac{2}{1-\nu_s}\sin^2\delta\cos^2\delta\sin^4\zeta + \cos^2\zeta$$
$$\mathcal{E}_2 \leq \mathcal{E}_2^+ = \left(\tfrac{2}{1-\nu_s}\cos^2\delta\cos^2\zeta + \sin^2\delta\right)\sin^2\zeta$$

3.3. Results

As expected, for both directions, we have:

$$0 < \mathcal{E}_\alpha^- \leq \mathcal{E}_\alpha^+ < 1$$

where $\mathcal{E} = 1$ corresponds to the Voigt upper bound and $\mathcal{E} = 0$ coprresponds to the Reuss lower bound. It should be emphasized that the derived bounds are independent of the shape ratio a_0/b_0. They are only functions of ν_s and the angles ζ and δ.

Fig. 6-(a,b) shows the normalized lower and upper bounds in direction 1 as functions of δ and ζ for $\nu_s = 0.4$. It is possible to give a simple interpretation for the lower bound $\mathcal{E}_1^-$. The corresponding trial stress has only one non-zero component: σ_{uu}. All the faces are subjected to uniaxial traction and compression in the $\underline{e}_u$ direction. This structural behavior can be compared to Warren truss beams (Fig. 7) where members are under alternative traction and compression. Hence, it is not surprising that the lower bound depends only on the member angle δ and is maximum for $\delta = \pi/4$ as for Warren truss beams. For most values of ζ and δ, $\mathcal{E}_1^-$ and $\mathcal{E}_1^+$ are not equal. However, for $\delta = \pi/4$ and $\cos^2\zeta = \nu_s$, they are coincident ($\mathcal{E}_1^- = \mathcal{E}_1^+ = \frac{1+\nu_s}{2}$). This means that, for this geometric configuration, the piecewise uniform trial strain and stress fields are the exact solutions for the transverse shear loading in direction 1.

Fig. 6-(c,d) show the normalized lower and upper bounds in direction 2. The trial stress field associated to $\mathcal{E}_2^-$ is mainly in-plane shear of the core walls as is the case for a honeycomb-like core. For $\zeta = \pi/2$, the pattern is prismatic and both bounds are equal to $\sin^2\delta$ which is an exact value for $\mathcal{E}_2$. Actually, prismatic cores are not used much in sandwich panels because they are not resistant enough. When decreasing ζ from $\pi/2$, the prismatic pattern becomes wavy and this waviness increases the faces' buckling strength under transverse shear loading in direction 1.

4. Finite element bounds

The analytical bounds suggested in the previous section are based on the piecewise uniform stress or strain assumption. In order to assess the validity of this assumption, a Finite Element analysis is conducted. The resulting numerical bounds will be compared to the analytical bounds.

4.1. The finite element model

The computation of the transverse shear moduli for both directions and both loading cases (stress and displacement) has been performed within the linear elasticity framework. The unit cell of Fig. 2 is chosen as a representative volume element.

Since faces are very thin, Kirchhoff shell elements are used. Four elements of the ABAQUS software (triangles P1 (STRI3), triangles P2 (STRI65), quadrangles P1 (S4R5) and quadrangles P2 (S8R5)) were

tested and compared through a convergence analysis (ABAQUS, 2007). Element S4R5 with a 441 node mesh gives accurate results for a low computation cost.

Boundary conditions involve both nodal displacements $\underline{U}$ and rotations $\underline{\Phi}$. For instance, $\underline{U}^{ABA'}$ and $\underline{\Phi}^{ABA'}$ refer respectively to nodal displacements and rotations along the edges AB and BA'.

Periodicity conditions in direction 1 and 2 have to be applied: ABA' matches $A''B''A'''$ and ADA'' matches $A'D'A'''$. As mentioned before, thanks to the symmetries of the unit cell there is no in-plane overall strain when applying tranverse shear loading. Hence, the following periodicity conditions are prescribed:

$$\underline{U}^{ABA'} = \underline{U}^{A''B''A'''}, \qquad \underline{\Phi}^{ABA'} = \underline{\Phi}^{A''B''A'''},$$

$$\underline{U}^{ADA''} = \underline{U}^{A'D'A'''}, \qquad \underline{\Phi}^{ADA''} = \underline{\Phi}^{A'D'A'''}.$$

The reader is referred to Sab (1996); Pradel and Sab (1998); Laroussi et al. (2002); Lachihab and Sab (2005); Florence and Sab (2006) for more details on periodic boundary conditions involving both nodal displacements and nodal rotations.

For the upper (respectively, lower) bound, the prescribed displacements (respectively, forces per unit length) are applied to the AB, BA', DC, CD', $A''B''$, $B''A'''$ edges. For the lower bound case, node A displacements and rotations are set to zero to prevent rigid motion.

Few detailed chevron folded core geometries are available in the open literature. Similar to Nguyen et al. (2005a), the following geometric parameters are investigated with $E_s = 3GPa$ and $\nu_s = 0.4$: $a_0 = 30\ mm$, $b_0 \in [20\ mm, 60\ mm]$, $t = 0.1mm$, $\delta = 72^\circ$, $\zeta = 34^\circ$. The analytical normalized bounds for these configurations are:

$$0.23 < \mathcal{E}_1 < 0.71,$$

$$0.09 < \mathcal{E}_2 < 0.35.$$

Fig. 8-(a,b,c) shows the stresses in the unit cell when submitted to the stress loading τ_1 for the case $a_0 = b_0 = 30mm$. At first sight, it is clear that the stresses are almost piecewise uniform in each face which is consistent with the assumption made for the analytical derivation of the lower bounds. Also, the stress distribution complies to the symmetries described in section 2. As expected, the main component is σ_{uu} as predicted by the Warren truss beam analogy.

Fig. 8-(d,e,f) shows the strains in the unit cell when submitted to the strain loading γ_1. Again, strains are approximately piecewise uniform in each face. Analytical estimations are $\frac{\varepsilon_{uu}}{\gamma_1} \approx 0.29$, $\frac{\varepsilon_{vv}}{\gamma_1} \approx 0.20$, $\frac{\varepsilon_{uv}}{\gamma_1} \approx 0.40$. FE fields seems consistent with this prediction.

Similar observations were made for the stress loading τ_2 and the strain loading γ_2 in direction 2.

4.2. Results

FE analysis has been performed also for several values of the shape ratio a_0/b_0 and for both loading directions. Results are shown on Fig. 9-(a,b).

For all shape ratios, the expected hierarchy between bounds is observed:

$$\mathcal{E}_\alpha^- < \mathcal{E}_\alpha^{-,\,FE} < \mathcal{E}_\alpha^{+,\,FE} < \mathcal{E}_\alpha^+. \tag{21}$$

For direction 1, on the one hand, the FE lower bound is really close to the analytical lower bound whatever the shape ratio is. This good agreement is consistent with the good uniformity of the stresses shown in Fig. 8-(a,b,c). On the other hand, the FE upper bound is dependent on the shape ratio. In fact, the computed strain fields are not perfectly piecewise uniform in this case. Fig. 8-(d,e,f). Moreover, it should be emphasized that the numerical FE bounds for direction 1 cover all the range between the analytical upper and lower bounds as the shape ratio varies. For direction 2, it is the lower bound which presents less uniform FE fields and is more sensitive to shape ratio. As expected, when the actual fields are almost piecewise uniform, then the analytical and numerical bounds are consistent.

One important conclusion of this study is that both FE and analytical bounds are loose for practical values of the shape ratio ($a_0/b_0 \in [0.5, 1.5]$). This means that the effective transverse shear moduli of the considered chevron pattern ($\delta = 72°$, $\zeta = 34°$) are sensitive to the the skin effect. According to Kelsey et al. (1958), this is due to the lack of consideration of the interaction between the skins and the core of the sandwich panel. Moreover, they indicate that the upper bound is relevant for sandwich panels with thick skins while the lower bound is relevant for thin skins.

4.3. Comparison with honeycomb

It is of interest to compare honeycomb geometries with chevron pattern.

For a regular honeycomb core with the same wall thickness, the use of piecewise uniform strain and stress in the core walls gives equal lower and upper bounds:

$$\mathcal{E}_1 = \mathcal{E}_2 = 0.5.$$

The normalized upper bounds for hexagonal honeycomb with a double wall in the glueing area are (Kelsey et al. (1958)):

$$\mathcal{E}_1^+ = \frac{1+\cos^2\theta}{2}, \qquad \mathcal{E}_2^+ = \frac{\sin^2\theta}{2}, \tag{22}$$

where the angle θ is a design parameter shown in Fig. 10. In order to compare chevron pattern to honeycomb, the sum $\Sigma = \mathcal{E}_1 + \mathcal{E}_2$ can be considered. Its upper bound for all honeycomb geometries is $\Sigma^+ = 1$ (Xu et al., 2001). However, for chevron pattern, it is:

$$\Sigma^+ = \left(\frac{2}{1-\nu_s}\cos^2\delta\sin^2\zeta + 1\right)\left(1 - \cos^2\delta\sin^2\zeta\right) \tag{23}$$

which reaches the maximum value:

$$\frac{(3-\nu_s)^2}{8(1-\nu_s)} \tag{24}$$

for

$$\cos^2\delta \sin^2\zeta = \frac{1+\nu_s}{4}. \tag{25}$$

Fig. 11-(a) shows Σ^+ as the function of ζ and δ for $\nu_s = 0.4$, and the continuous set of (ζ, δ) for which Σ^+ reaches its maximum value. On Fig. 12 the maximum value of Σ^+ versus ν_s is plotted. Thus, considering Σ^+, the chevron pattern can potentially outperform honeycomb by $\simeq 40\%$ for usual values of ν_s.

In Fig. 11-(b) the FE computed sum of upper bounds $\Sigma^{+,FE}$ is plotted for $a_0/b_0 = 1$. As expected FE upper bounds are lower than analytical upper bounds. The domain where chevron pattern outperforms honeycomb geometries ($\Sigma^{+,FE} > 1$) is smaller but still includes geometries that can be manufactured. Yet, $\Sigma^{+,FE} \simeq 0.65$ for the geometry considered in Nguyen et al. (2005a).

5. Discussion

The main reason for the gap observed between bounds, even with FE computations, is the lack of knowledge on the actual effect of shear forces on plates. Since Reissner (1945) we know that local tranverse shear is parabolic through the thickness in a homogeneous plate. However, when considering anisotropic laminated plates, it is difficult to approximate the actual transverse shear stress distribution. To overcome this diffficulty, Mindlin (1951) suggested to introduce shear correction factors, which improved the accuracy of the deflection prediction but did not provided the actual transverse shear stress distribution. Numerous proposals have been made to improve stress estimation and were reviewed by Reddy (1989) and Carrera (2002). This issue becomes critical when considering heterogeneous periodic plates such as honeycomb and chevron pattern sandwich panels.

Most of the approaches suggested for sandwich panels rely on the following steps. First, the heterogeneous core is homogenized, and replaced with an equivalent homogeneous layer. Second, the First Order Shear Deformation Theory (FOSDT) is applied to derive the transverse shear stiffness of the obtained laminated plate. To do this, the transverse shear strain is assumed uniform through the thickness. Two difficulties arise from this two step method.

Firstly, the actual boundary conditions replacing the effect of the skins on the core are unknown. Imposing uniform displacements or uniform forces gives bounds for the homogenized constitutive behavior of the heterogeneous core. As it is illustrated in this paper, these bounds may be loose. This is the main drawback of the two step approach.

Secondly, as previously mentioned, the application of FOSDT necessitates the computation of shear correction factors. However shear correction factors depend on the ply configuration. In the case of heterogeneous plates, the concept of shear corerection factor is even more fuzzy. The work of Buannic et al. (2003) points out limitations of the shear correction factor approach.

One way has been suggested to overcome these difficulties in the case of honeycomb sandwich panels. It consists in refining the analysis on the connection between the skins and the core, as suggested by Hohe and Becker (2001) and Chen and Davalos (2005). In these papers the incompatibility between the skins and the core average displacement is treated as an edge effect relatively to the ratio between the cell width and the core thickness. Following a completely different path, Lebée and Sab (2010) suggested a model which enables the consideration of such incompatibilities and edge effects in more general configurations. Yet this kind of approach is relevant only for honeycombs. Unlike honeycombs, the chevron pattern has no scale separation between the cell width and the core thickness.

A second way to improve the estimation of the transverse shear stiffness is to reconsider globally the effect of shear forces on the sandwich panel. This was done by Hohe (2003) and Cecchi and Sab (2007) among others. Hohe (2003), followed by Pahr and Rammerstorfer (2006), presented a direct homogenization scheme assuming *ad hoc* boundary conditions on the representative volume element, including skins. When including skins, Hohe (2003) overcomes the difficulty of choosing the actual boundary conditions that should be used in the two step method. However, applying this method to a homogeneous plate leads to a uniform stress distribution which contradicts Reissner (1945)'s prediction and overestimates transverse shear stiffness (hG instead of $5/6hG$). The reason why Hohe (2003) method is efficient for sandwich panels comes from a constrast assumption. In sandwich panels, the core is allways much more compliant than the skins. In this specific case it is possible to assume a uniform distribution of shear strains through the core thickness. Yet, in practical applications, the contrast assumption is not always fullfilled which limits the validity of this method. Another proposal, made by Cecchi and Sab (2007) (as well as, Cecchi and Sab (2004); Nguyen et al. (2005b); Cecchi and Sab (2007); Nguyen et al. (2007, 2008)), is based on Whitney (1972) work on the derivation of shear correction factors for laminates. This seminal work is extended to heterogeneous plates thanks to an energetic equivalence. It consists in using the Reissner-Mindlin equilibrium equation $M_{\alpha\beta,\beta} = Q_\alpha$ in the cylindrical bending case in order to derive the actual 3D stress field generated by shear forces. This method does not make an *a priori* assumption on transverse shear strain or stress. It is currently under investigation for application to sandwich panels.

6. Conclusion

For an out-of-plane loaded sandwich panel with stiff skins (0.6 mm of CFRP for instance), small slenderness ratio (10 for example) and usual chevron folded core thickness (0.1 mm of impregnated aramid paper), the deflection is almost proportional to the effective transverse shear moduli of the chevron folded core. In this paper, Kelsey et al. (1958) approach has been used to derive analytical and numerical upper bounds for these moduli. For some pattern geometries, the exact fields have been obtained. Moreover, it has been shown that for some geometries, the chevron folded cores are stiffer than honeycomb-like cores (lower bounds

for the chevron core are higher than upper bounds for honeycombs). Finally, this work sets the path for the derivation of analytical bounds for other folded core geometries such as the M-type core (Heimbs et al., 2007).

However, the bounds obtained for the already existing pattern geometries (Nguyen et al., 2005a), $\delta = 72°$, $\zeta = 34°$, are too loose (more than 100% discrepancy). Kelsey et al. (1958) already discussed this difficulty in the context of honeycomb core structures, but it is even more pronounced in the case of chevron structures.

In the case of honeycomb-like cores, the discrepancy between bounds has been identified as a skin effect (Hohe and Becker, 2001; Xu and Qiao, 2002; Chen and Davalos, 2005) and correlated to the ratio between the cell width and the core thickness. In the case of chevron folded core, the large discrepancy between the bounds has still no explanation and necessitates more refined models able to take into account the interaction between the skins and the core.

Appendix

The components of the local basis are given by:

$$(\underline{e}_u^1, \underline{e}_v^1, \underline{e}_w^1) = \underline{\underline{\mathcal{T}}} = \begin{pmatrix} \cos\delta & \sin\zeta\cos\delta & -\sin\delta\sin\zeta \\ 0 & \sin\zeta & \cos\zeta \\ \sin\delta & -\cos\delta\cos\zeta & \cos\delta\sin\zeta \end{pmatrix}_{(\underline{e}_1,\underline{e}_2,\underline{e}_3)} \tag{26}$$

$$(\underline{e}_u^2, \underline{e}_v^2, \underline{e}_w^2) = \underline{\underline{\mathcal{N}}}\,\underline{\underline{\mathcal{T}}}\,\underline{\underline{\mathcal{N}}} = \begin{pmatrix} \cos\delta & -\sin\zeta\cos\delta & -\sin\delta\sin\zeta \\ 0 & \sin\zeta & -\cos\zeta \\ \sin\delta & \cos\delta\cos\zeta & \cos\delta\sin\zeta \end{pmatrix}_{(\underline{e}_1,\underline{e}_2,\underline{e}_3)} \tag{27}$$

$$(\underline{e}_u^3, \underline{e}_v^3, \underline{e}_w^3) = \underline{\underline{\mathcal{S}}}\,\underline{\underline{\mathcal{N}}}\,\underline{\underline{\mathcal{T}}}\,\underline{\underline{\mathcal{N}}}\,\underline{\underline{\mathcal{S}}} = \begin{pmatrix} \cos\delta & -\sin\zeta\cos\delta & \sin\delta\sin\zeta \\ 0 & \sin\zeta & \cos\zeta \\ -\sin\delta & -\cos\delta\cos\zeta & \cos\delta\sin\zeta \end{pmatrix}_{(\underline{e}_1,\underline{e}_2,\underline{e}_3)} \tag{28}$$

$$(\underline{e}_u^4, \underline{e}_v^4, \underline{e}_w^4) = \underline{\underline{\mathcal{S}}}\,\underline{\underline{\mathcal{T}}}\,\underline{\underline{\mathcal{S}}} = \begin{pmatrix} \cos\delta & \sin\zeta\cos\delta & \sin\delta\sin\zeta \\ 0 & \sin\zeta & -\cos\zeta \\ -\sin\delta & \cos\delta\cos\zeta & \cos\delta\sin\zeta \end{pmatrix}_{(\underline{e}_1,\underline{e}_2,\underline{e}_3)} \tag{29}$$

References

ABAQUS, 2007. ABAQUS/Standard user's manual, version 6.7. ABAQUS.

Basily, B., Elsayed, A., (03/10/2006). Technology for continuous folding of sheet materials. US patent: US 7, 115, 089 B2

Basily, B., Elsayed, A., 2004a. A continuous folding process for sheet materials. International Journal of Materials and Product Technology 21, 217–238.

Basily, B., Elsayed, E., 2004b. Dynamic axial crushing of multi-layer core structures of folded chevron patterns. International Journal of Materials and Product Technology 21, 169–185.

Buannic, N., Cartraud, P., Quesnel, T., 2003. Homogenization of corrugated core sandwich panels. Composite Structures 59 (3), 299–312.

Caillerie, D., 1984. Thin elastic and periodic plates. Mathematical Methods in the Applied Sciences 6 (2), 159 – 191.

Carrera, E., 2002. Theories and finite elements for multilayered, anisotropic, composite plates and shells. Archives Of Computational Methods In Engineering 9 (2), 87–140.

Cecchi, A., Sab, K., 2004. A comparison between a 3d discrete model and two homogenised plate models for periodic elastic brickwork. International Journal of Solids and Structures 41 (9-10), 2259–2276.

Cecchi, A., Sab, K., 2007. A homogenized reissner-mindlin model for orthotropic periodic plates: Application to brickwork panels. International Journal of Solids and Structures 44 (18-19), 6055–6079.

Chen, A., Davalos, J. F., 2005. A solution including skin effect for stiffness and stress field of sandwich honeycomb core. International Journal of Solids and Structures 42 (9-10), 2711 – 2739.

Cote, F., Biagi, R., Bart-Smith, H., Deshpande, V. S., May 2007. Structural response of pyramidal core sandwich columns. International Journal of Solids and Structures 44 (10), 3533–3556.

Florence, C., Sab, K., 2006. A rigorous homogenization method for the determination of the overall ultimate strength of periodic discrete media and an application to general hexagonal lattices of beams. European Journal of Mechanics - A/Solids 25 (1), 72 – 97.

Gibson, L. J., Ashby, M. F., 1988. Cellular solids. Pergamon Press.

Heimbs, S., 2009. Virtual testing of sandwich core structures using dynamic finite element simulations. Computational Materials Science 45 (2), 205 – 216.

Heimbs, S., Mehrens, T., Middendorf, P., Maier, A., Schumacher, M., 2006. Numerical determination of the nonlinear effective mechanical properties of folded core structures for aircraft sandwich panels. 6^{th} European LS DYNA User's Conference.

Heimbs, S., Middendorf, P., Kilchert, S., Johnson, A., Maier, M., Nov. 2007. Experimental and numerical analysis of composite folded sandwich core structures under compression. Applied Composite Materials 14 (5), 363–377.

Hohe, J., Oct. 2003. A direct homogenisation approach for determination of the stiffness matrix for microheterogeneous plates with application to sandwich panels. Composites Part B: Engineering 34 (7), 615–626.

Hohe, J., Becker, W., May 2001. A refined analysis of the effective elasticity tensor for general cellular sandwich cores. International Journal of Solids and Structures 38 (21), 3689–3717.

Hohe, J., Becker, W., 2002. Effective stress-strain relations for two-dimensional cellular sandwich cores: Homogenization, material models, and properties. Applied Mechanics Reviews 55 (1), 61–87.

Kehrle, R., Airbus, D., (27/05/2004). Method for the production of a sandwich structure for a sandwich composite. World Patent: WO 2004/043685

Kelsey, S., Gellatly, R., Clark, B., 1958. The shear modulus of foil honeycomb cores: A theoretical and experimental investigation on cores used in sandwich construction. Aircraft Engineering and Aerospace Technology 30 (10), 294 – 302.

Kintscher, M., Karger, L., Wetzel, A., Hartung, D., May 2007. Stiffness and failure behaviour of folded sandwich cores under combined transverse shear and compression. Composites Part A: Applied Science and Manufacturing 38 (5), 1288–1295.

Kling, D. H., (30/08/2005). Paterning technology for folded sheet structures. US Patent: US 6,935, 997 B2

Lachihab, A., Sab, K., Jun. 2005. Aggregate composites: a contact based modeling. Computational Materials Science 33 (4), 467–490.

Laroussi, M., Sab, K., Alaoui, A., 2002. Foam mechanics: nonlinear response of an elastic 3d-periodic microstructure. International Journal of Solids and Structures 39 (13-14), 3599 – 3623.

Lebée, A., Sab, K., Apr. 2010. A cosserat multiparticle model for periodically layered materials. Mechanics Research Commu-

nications 37 (3), 293–297.

Mindlin, R., 1951. Influence of rotatory inertia and shear on flexural motions of isotropic, elastic plates. Journal of Applied Mechanics 18, 31–38.

Nguyen, M., Jacombs, S., Thomson, R., Hachenberg, D., Scott, M., Feb. 2005a. Simulation of impact on sandwich structures. Composite Structures 67 (2), 217–227.

Nguyen, T. K., Sab, K., Bonnet, G., 2007. Shear correction factors for functionally graded plates. Mechanics of Advanced Materials and Structures 14 (8), 567–575.

Nguyen, T.-K., Sab, K., Bonnet, G., Mar. 2008. First-order shear deformation plate models for functionally graded materials. Composite Structures 83 (1), 25–36.

Nguyen, V.-T., Caron, J.-F., Sab, K., 2005b. A model for thick laminates and sandwich plates. Composites Science and Technology 65 (3-4), 475 – 489.

Pahr, D. H., Rammerstorfer, F. G., Apr. 2006. Buckling of honeycomb sandwiches: Periodic finite element considerations. Cmes-Computer Modeling In Engineering & Sciences 12 (3), 229–241.

Pradel, F., Sab, K., 1998. Homogenization of discrete media. Journal De Physique. IV : JP 8 (8), 317 – 324.

Reddy, J. N., 1989. On refined computational models of composite laminates. International Journal For Numerical Methods In Engineering 27 (2), 361–382.

Reissner, E., 1945. The effect of transverse shear deformation on the bending of elastic plates. Journal of Applied Mechanics 12, 68–77.

Reissner, E., 1985. Reflections on the theory of elastic plates. Applied Mechanics Reviews 38 (11), 1453 – 1464.

Sab, K., 1996. Microscopic and macroscopic strains in a dense collection of rigid particles. Comptes Rendus de l'Academie Des Sciences Serie II Fascicule B-Mecanique Physique Chimie Astronomie 322 (10), 715–721.

Wadley, H., 2002. Cellular metals manufacturing. Advanced Engineering Materials 4 (10), 726–733.

Whitney, J., 1972. Stress analysis of thick laminated composite and sandwich plates. Journal of Composite Materials 6 (4), 426–440.

Wicks, N., Hutchinson, J. W., Jul. 2001. Optimal truss plates. International Journal of Solids and Structures 38 (30-31), 5165–5183.

Xu, X. F., Qiao, P., 2002. Homogenized elastic properties of honeycomb sandwich with skin effect. International Journal of Solids and Structures 39 (8), 2153 – 2188.

Xu, X. F., Qiao, P., Davalos, J. F., 2001. Transverse shear stiffness of composite honeycomb core with general configuration. Journal of Engineering Mechanics 127 (11), 1144–1151.

Zakirov, I., Alekseev, K., Movchan, G., 2008. Influence of coating thickness on geometric parameters of a chevron core. Russian Aeronautics 51 (3), 326 – 329.

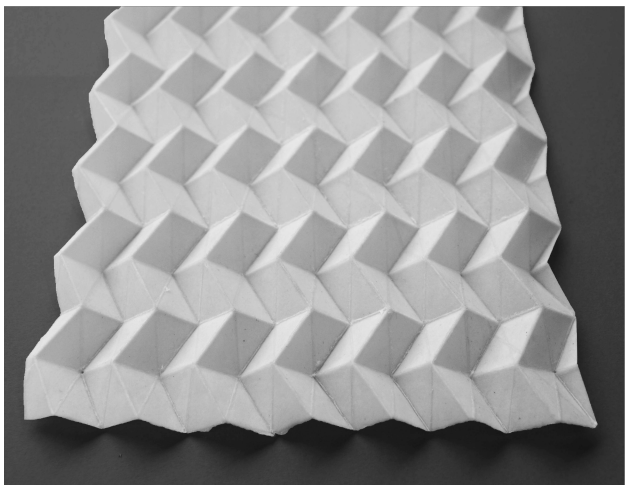

Figure 1: Chevron folded paper.

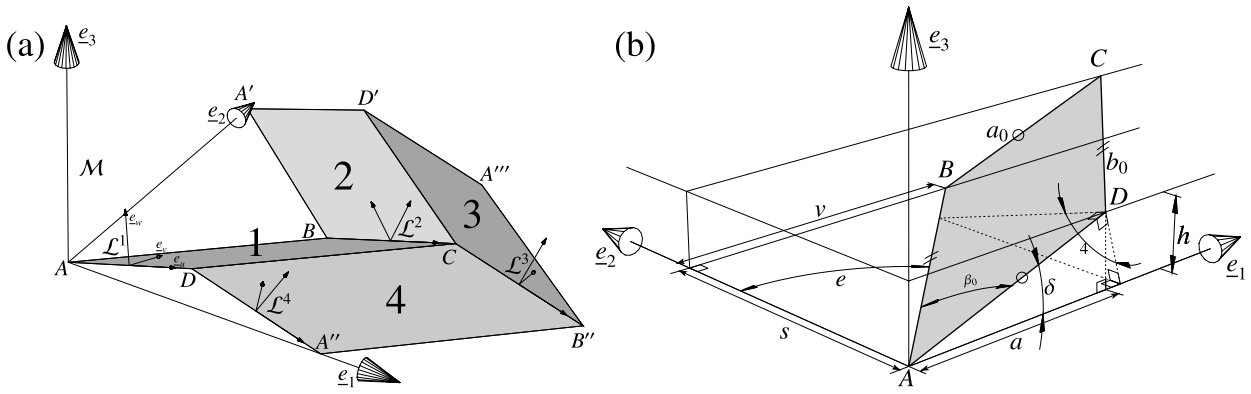

Figure 2: The four elementary faces of the pattern (a) and Face 1 orientation (b).

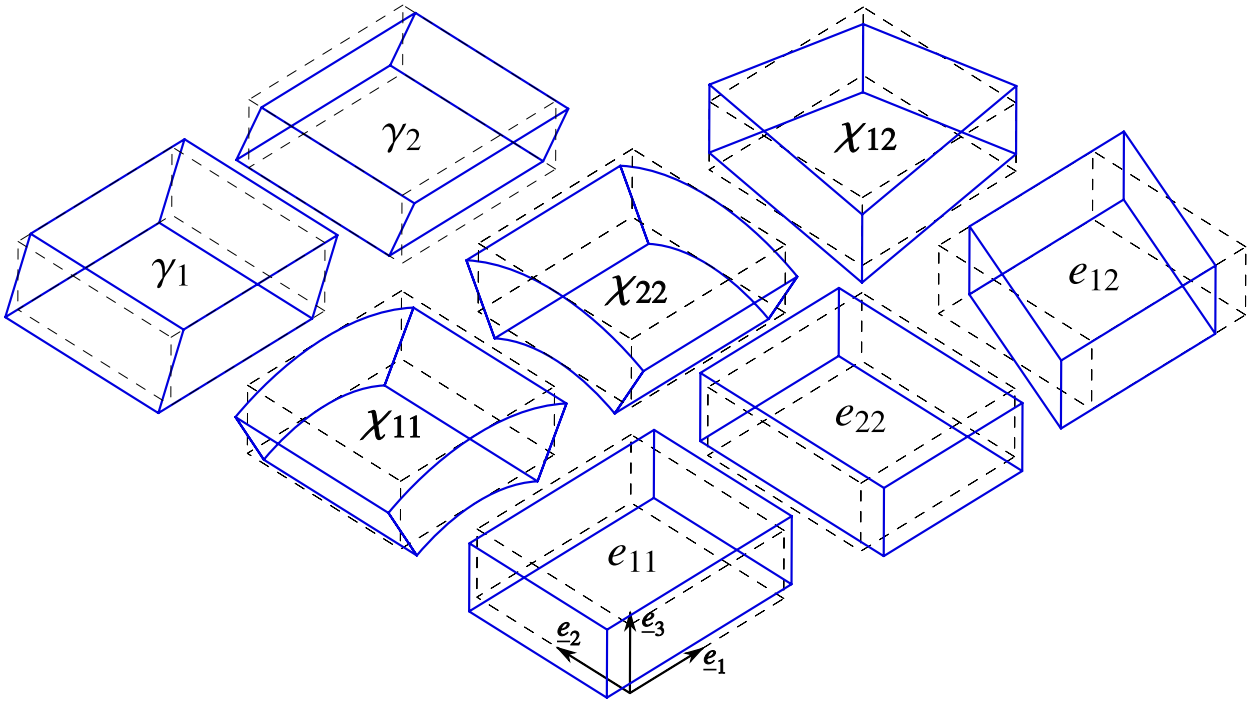

Figure 3: Reissner-Mindlin generalized strains

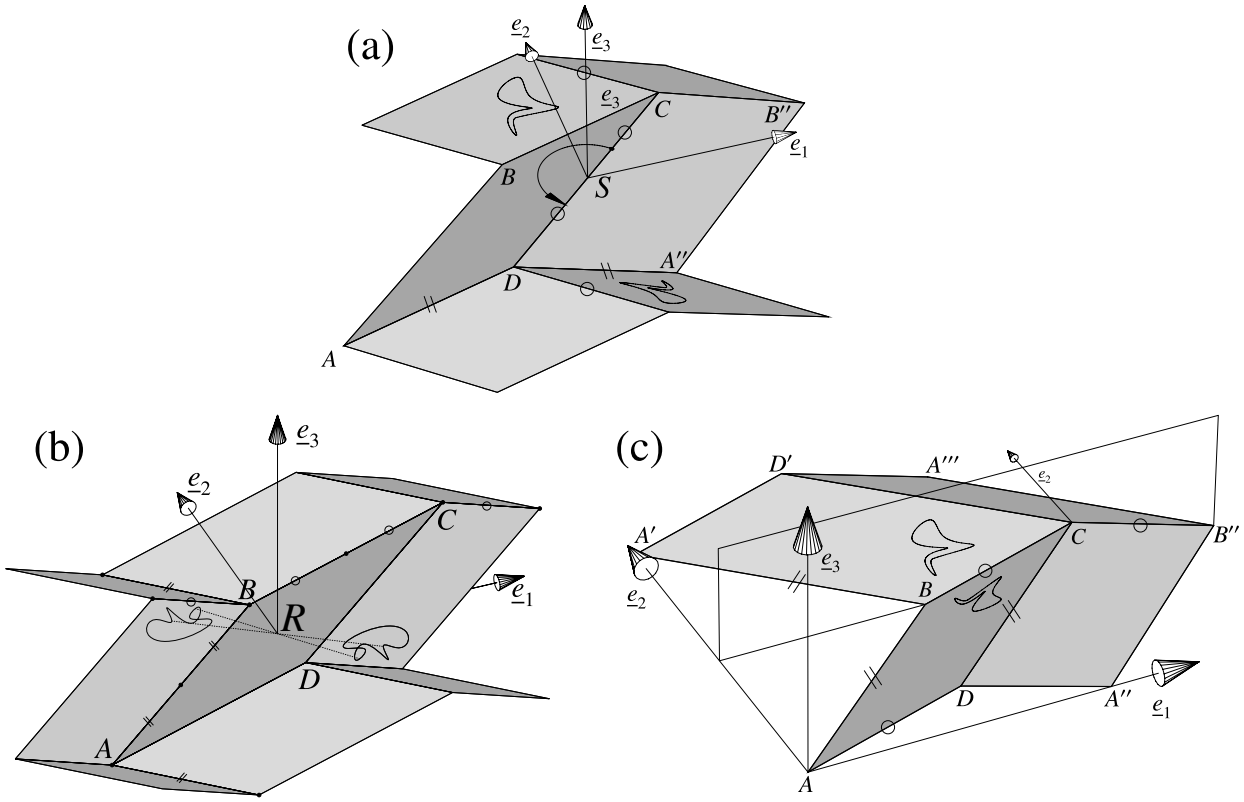

Figure 4: Rotational symmetry with respect to $(S, \underline{e}_3)$ (a). Central symmetry with respect to point R (b). Symmetry with respect to $(B, \underline{e}_1, \underline{e}_3)$ plane (c). axis

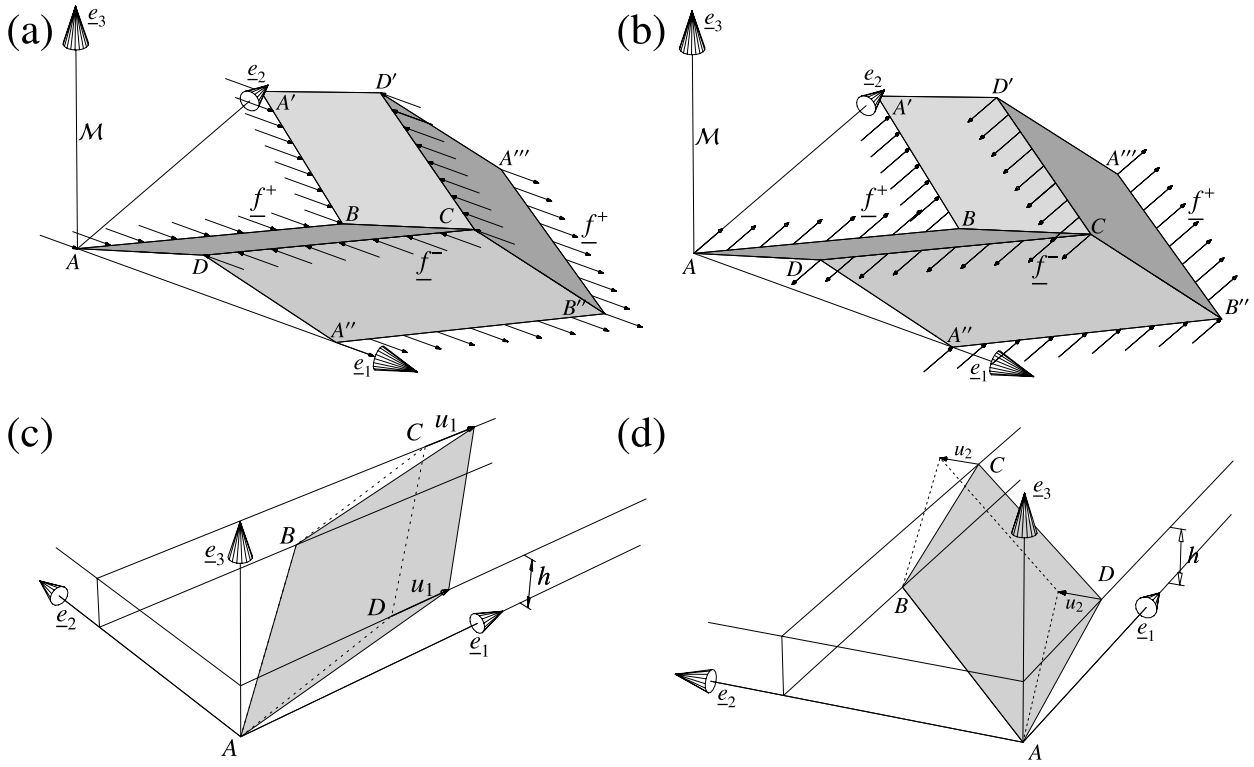

Figure 5: Stress load in direction 1: (a) and in direction 2: (b). Face 1 displacement in direction 1: (c) and in direction 2: (d).

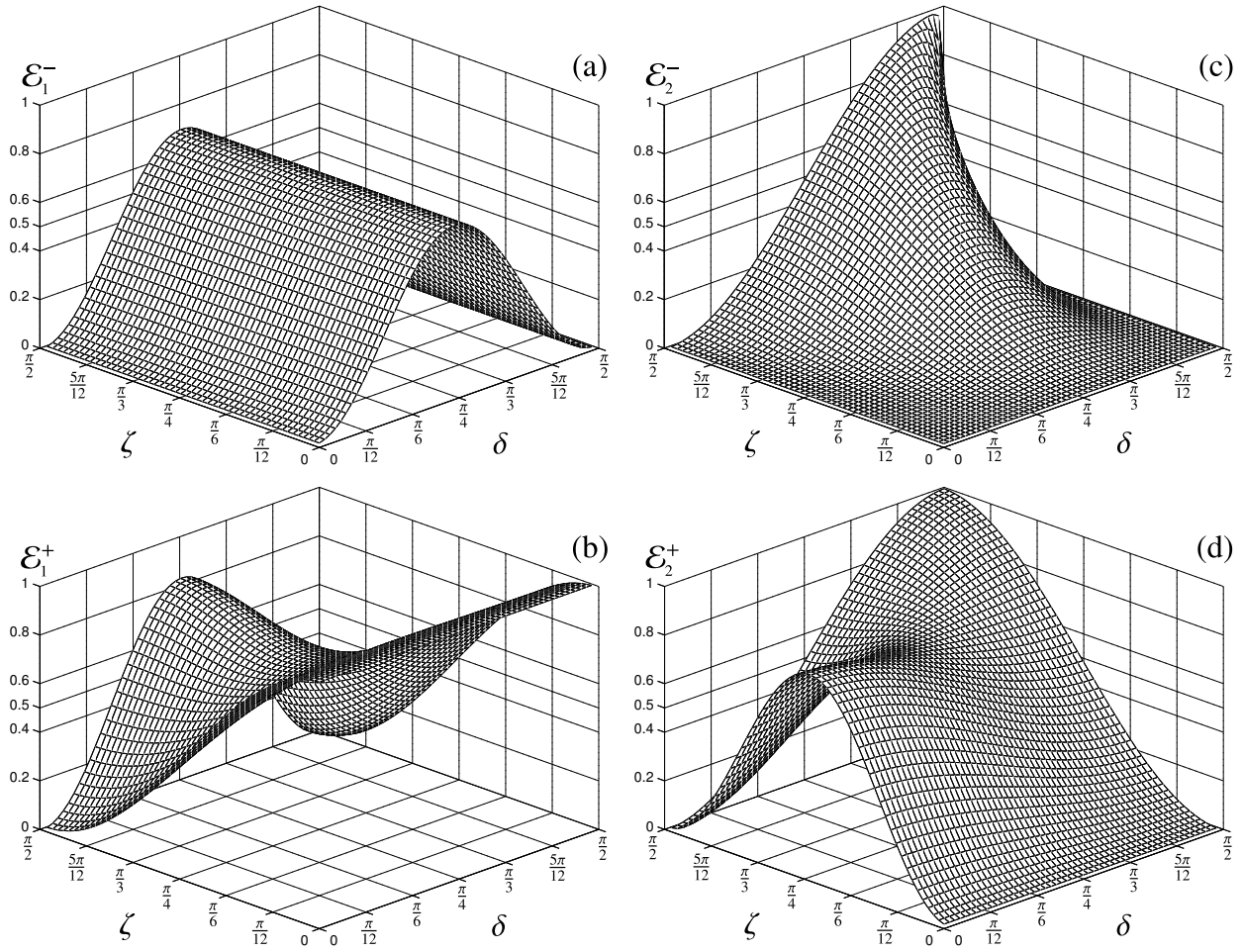

Figure 6: Analytical bounds $\mathcal{E}$ for both directions as the function of ζ and δ for $\nu_s = 0.4$ and $a_0/b_0 = 1$.

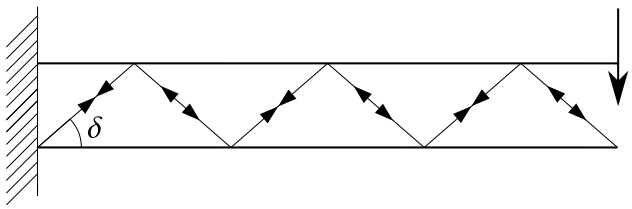

Figure 7: Warren truss beam.

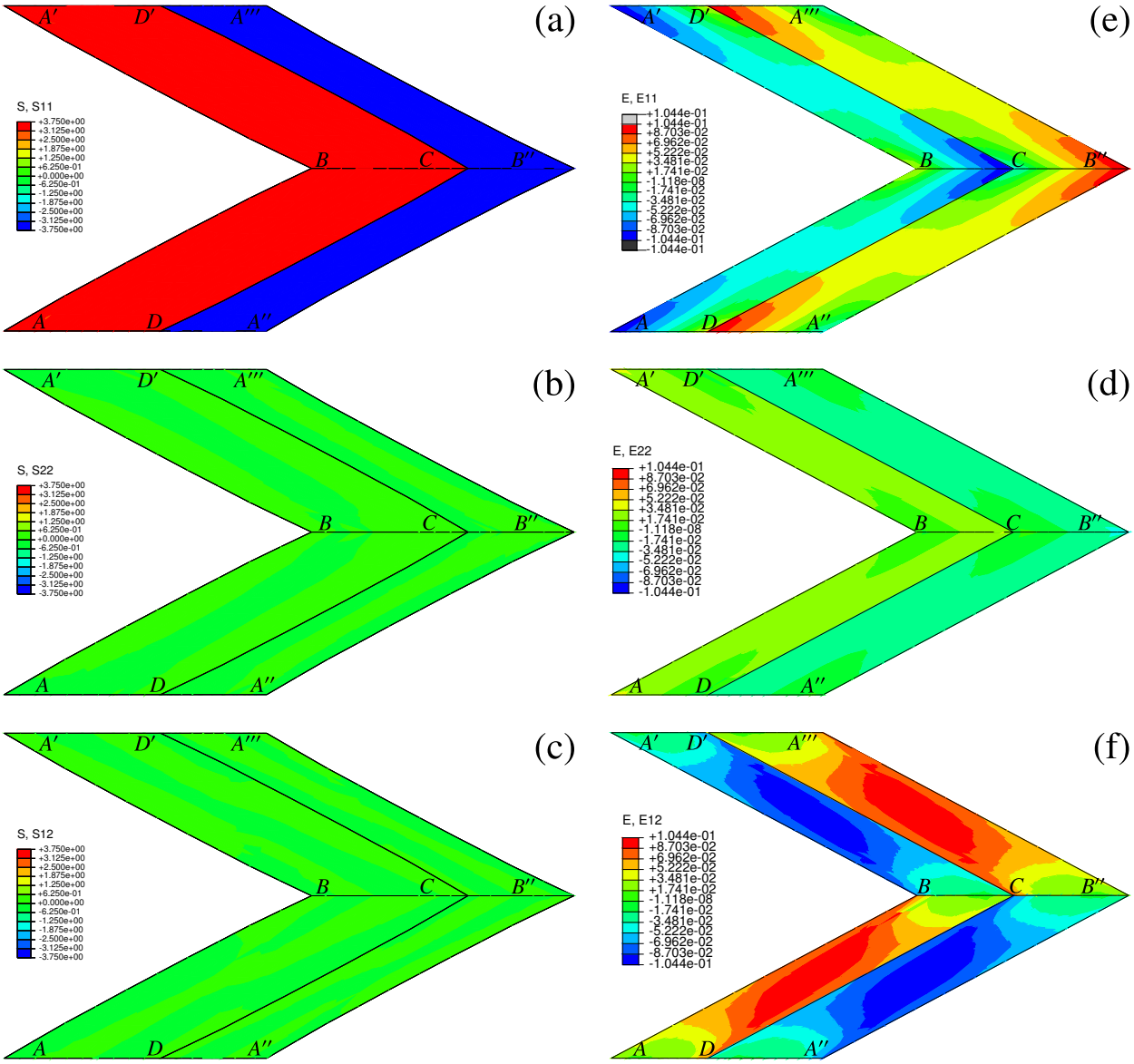

Figure 8: Membrane stresses for τ_1 load, $\delta = 72^\circ$, $\zeta = 34^\circ$ ((a): σ_{uu}, (b): σ_{vv}, (c): σ_{uv}) and membrane strains for γ_1 load, $\delta = 72^\circ$, $\zeta = 34^\circ$ ((d): ε_{uu}, (e): ε_{vv}, (f): ε_{uv})

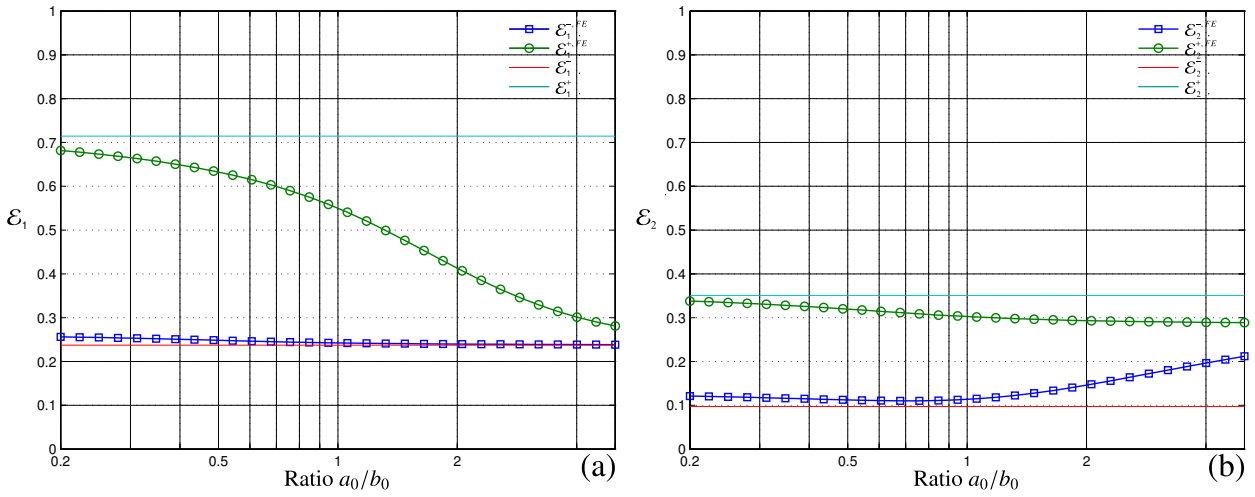

Figure 9: Bounds versus a_0/b_0 for $\delta = 72^\circ$, $\zeta = 34^\circ$ and $\nu_s = 0.4$ in both directions.

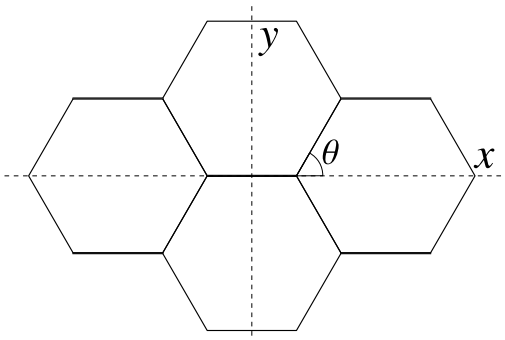

Figure 10: Honeycomb angle.

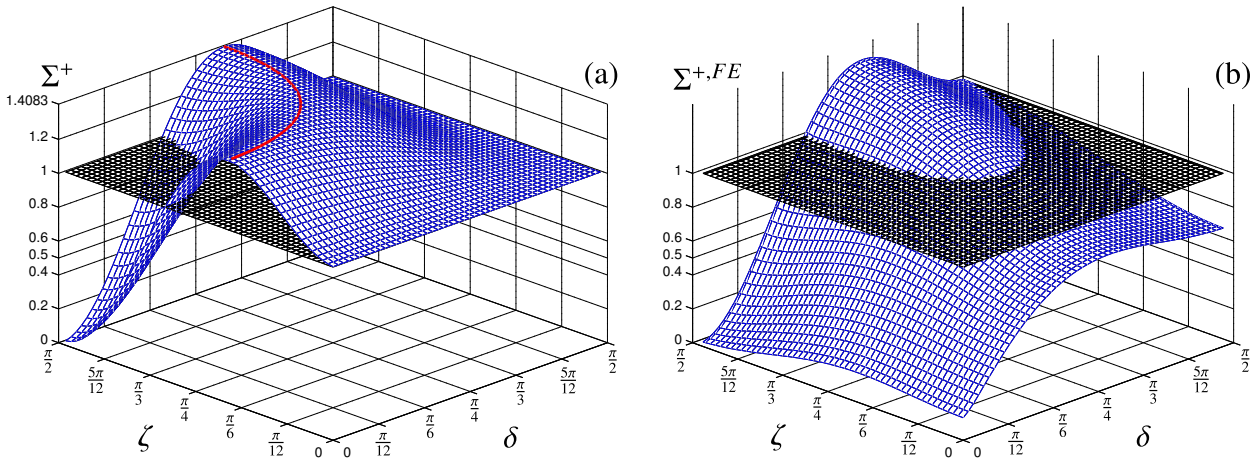

Figure 11: Σ^+ and $\Sigma^{+,FE}$ as the function of ζ and δ for $\nu_s = 0.4$ and $a_0/b_0 = 1$.

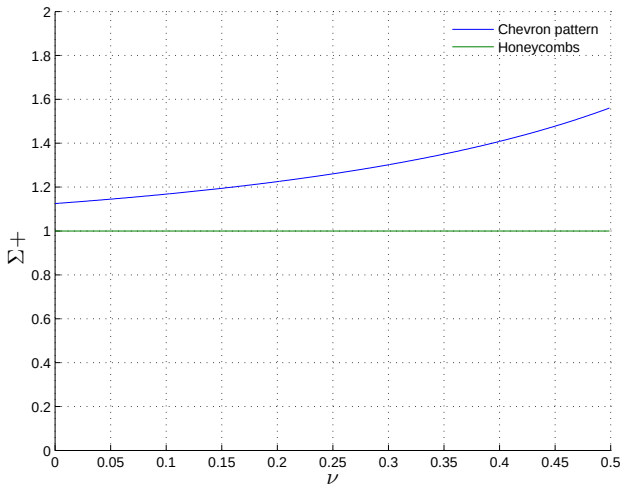

Figure 12: Maximum value of Σ^+ for honeycombs and chevron pattern versus Poisson's ratio, ν_s.